

Effect of Grain Statistics on Micromechanical Modeling: The Example of Additively Manufactured Materials Examined by Electron Backscatter Diffraction

Abhishek Biswas,* Mahesh R. G. Prasad, Napat Vajragupta, Aleksander Kostka, Thomas Niendorf, and Alexander Hartmaier

Micromechanical modeling is one of the prominent numerical tools for the prediction of mechanical properties and the understanding of deformation mechanisms of metals. As input parameters, it uses data obtained from microstructure characterization techniques, among which the electron backscatter diffraction (EBSD) technique allows us to understand the nature of microstructural features, that are usually described by statistics. Because of these advantages, the EBSD dataset is widely used for synthetic microstructure generation. However, for the statistical description of microstructural features, the population of input data must be considered. Preferably, the EBSD measurement area must be sufficiently large to cover an adequate number of grains. However, a comprehensive study of this measurement area with a crystal plasticity finite element method (CPFEM) framework is still missing although it would considerably facilitate information exchange between experimentalists and simulation experts. Herein, the influence of the EBSD measurement area and the number of grains on the statistical description of the microstructural features and studying the corresponding micromechanical simulation results for 316L stainless steel samples produced by selective laser melting is investigated.

questions. Before these models can be used, calibrating and verifying them with experiments is particularly important.

The heterogeneity of polycrystalline metals poses a challenge in modeling them, which can be overcome by micromechanical modeling^[1] for predicting the deformation mechanisms and incorporating plastic behavior and other mechanical properties like crystallographic orientation evolution. Micromechanical modeling has been well established in recent decades, and it has been used to study the deformation mechanisms of several metallic materials.^[2–4] In some recent works, it has also been extended to polycrystalline materials produced by the selective laser melting technique.^[5,6]


For micromechanical modeling, a statistical representation of the real microstructure is required, capturing key microstructural features like grain size, shape, and texture, for producing a synthetic microstructure. This synthetic microstructure

should be large enough to represent the bulk material properties as well as remain computationally efficient. The microstructural features mentioned earlier are determined experimentally using various characterization techniques. Out of the many techniques available, the characterization of polycrystalline metals with electron backscatter diffraction (EBSD) provides a deep insight into the crystallographic orientations and the grain structures of the microstructure, and it allows large regions of a bulk sample to be readily analyzed, which is feasible

1. Introduction

Both experiments and numerical modeling are important for the scientific investigation of materials. Experimental techniques provide in-depth information on the elementary mechanisms contributing to the performance of the material, but in many circumstances, these techniques encounter practical limitations or are very expensive. In such cases, modeling of material behavior numerically can be useful in providing solutions for scientific

A. Biswas, M. R. G. Prasad, Dr. N. Vajragupta, Prof. A. Hartmaier
Interdisciplinary Centre for Advanced Materials Simulation (ICAMS)
Ruhr-Universität Bochum
Universitätsstr. 150, 44801 Bochum, Germany
E-mail: abhishek.biswas@rub.de

 The ORCID identification number(s) for the author(s) of this article can be found under <https://doi.org/10.1002/adem.201901416>.

© 2020 The Authors. Published by WILEY-VCH Verlag GmbH & Co. KGaA, Weinheim. This is an open access article under the terms of the Creative Commons Attribution License, which permits use, distribution and reproduction in any medium, provided the original work is properly cited.

DOI: 10.1002/adem.201901416

Dr. A. Kostka
Center for Interface Dominated High Performance Materials (ZGH)
Institute of Materials
Ruhr-Universität Bochum
Universitätsstr. 150, 44801 Bochum, Germany

Prof. T. Niendorf
Institut für Werkstofftechnik
Universität Kassel
Mönchebergstr. 3, 34125 Kassel, Germany

with recent developments in instrumentations for rapid and automated scans of the material.^[7]

Several studies were summarized in the study by Randle and Engler,^[8] which focuses on the representativeness of the EBSD in terms of the number of single grain orientations. From these studies, another key microstructural feature like texture and its representativeness is related to the number of grains captured from EBSD measurement. For the case of cubic crystal-orthonormal sample symmetry, $\approx 10\,000$ grains must be captured in the EBSD measurement to properly characterize texture in the material. This is also supported by the experimental study conducted in the study by Wright et al.,^[9] wherein the orientation distribution function (ODF) from EBSD is compared with X-ray diffraction measurements. Another study focusing on a weaker texture^[10] suggests several tens of thousands of grains. Similarly in the study by Davut and Zaefferer,^[11] the representativeness of the EBSD data for phase fraction determination in transformation induced plasticity steels is studied.

EBSD data have often been fed as an input for micromechanical simulation, as reported by several studies.^[12–14] At the center of micromechanical modeling, a representative volume element (RVE) is used for predicting material behavior. The representativeness of the RVE is particularly important with regard to size and statistical descriptions of essential microstructural features. To achieve numerical efficiency, Nakamachi et al.,^[12] Brands et al.,^[13] and Pélissou et al.^[15] presented methods to optimize the RVE size while maintaining the representativeness. Generally, it is well known that in any statistical analysis, the data sample size should be large enough to avoid any artifacts/bias, which is also applicable for experimental data used for micromechanical modeling.

Considering these studies, it can be concluded that the representativeness of the EBSD data is very important for a micromechanical modeling approach. However, there has been

no study which suggests an experimental strategy to obtain the representative EBSD data for micromechanical simulations. In this work, we hence put an emphasis on a comprehensive study to understand the effect of EBSD data on the results of a micromechanical model within the crystal plasticity finite element model (CPFEM) framework. In this context, we focus on suggesting an adequate number of grains to be covered by EBSD measurement, yielding representative micromechanical simulation results.

For this study, a large EBSD scan (**Figure 1**) ($\approx 4 \times 5 \text{ mm}^2$) is performed on additively manufactured 316L stainless steel. First, the microstructural features like texture and grain size are extracted from the large EBSD dataset to generate a synthetic microstructure. This microstructure is then used in the CPFEM to predict the mechanical behavior of the material numerically. The crystal plasticity (CP) parameters are calibrated with the data obtained from experimental uniaxial compression tests, as described in the Section 3.3.

In the next step, further several smaller EBSD scans are randomly created from the large EBSD dataset by making crop windows of sizes $0.5 \text{ mm} \times 0.5 \text{ mm}$, $1 \text{ mm} \times 1 \text{ mm}$, $2 \text{ mm} \times 2 \text{ mm}$, and $3 \text{ mm} \times 3 \text{ mm}$. The cropped areas are saved as new EBSD data, essentially representing the same material but capturing a smaller area. The microstructural features are extracted from the smaller EBSD scans and used to generate synthetic microstructures. Finally, finite element (FE) simulations are conducted

Table 1. Grain dimensions in the form of mean equivalent diameter μ_{dia} in mm and mean aspect ratio μ_{AR} estimated from the large EBSD dataset (cf. Figure 1) and cropped EBSD datasets (cf. Figure 2).

Model	Large EBSD dataset		3 mm × 3 mm		2 mm × 2 mm		1 mm × 1 mm		0.5 mm × 0.5 mm	
	μ_{dia}	μ_{AR}	μ_{dia}	μ_{AR}	μ_{dia}	μ_{AR}	μ_{dia}	μ_{AR}	μ_{dia}	μ_{AR}
1	0.019	2.5	0.019	2.6	0.020	2.6	0.020	2.6	0.021	2.6
2			0.019	2.4	0.020	2.6	0.020	2.6	0.017	2.5
3			0.019	2.6	0.020	2.6	0.020	2.5	0.020	2.6
4					0.019	2.5	0.019	2.2	0.019	2.5
5					0.019	2.6	0.019	2.6	0.019	2.5
6							0.019	2.6	0.018	2.5
7							0.020	2.5	0.020	2.5
8							0.018	2.5	0.019	2.4
9							0.019	2.5	0.020	2.5
10							0.019	2.5	0.018	2.5
11									0.018	2.7
12									0.019	2.7
13									0.020	2.4
14									0.019	2.2
15									0.019	2.4
16									0.018	2.6
17									0.019	2.8
18									0.017	2.9
19									0.020	2.4
20									0.020	2.2

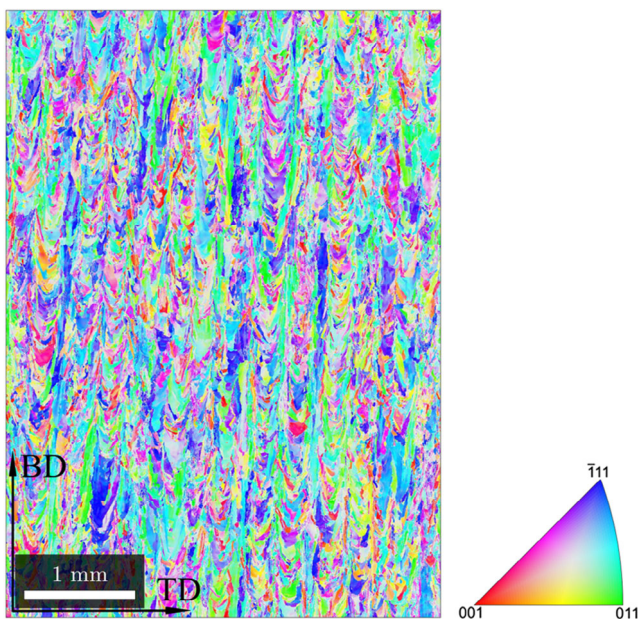


Figure 1. EBSD map (referred to as large EBSD from now) after denoising and the orientation triangle.

by applying precalibrated CP parameters to predict the mechanical response of the different synthetic microstructures under uniaxial compression. The results from the simulations of the smaller scan areas are compared with those of the large EBSD dataset, to provide an overview of the EBSD scan area's influence on the numerical model results.

2. Material Characterization and Analysis

The samples of 316L stainless steel used in this study were manufactured by the selective laser melting technique, using a system with a nominal laser power of 400 W. The laser scanning strategies followed the standard parameters, e.g., detailed in a previous

study.^[16] The samples were processed from prealloyed 316 L powder that had been gas atomized. It was revealed in numerous studies, e.g., in a study by Riemer et al.^[16], that the chemical composition of samples processed by selective laser melting in adequate process windows does not differ from the composition of conventionally processed sheet material. In that previous study^[16] processing followed the same steps as in present work and the chemical composition was reported to be (in wt%) 0.018 C, 17.030 Cr, 2.270 Mo, 10.520 Ni, Fe = balance. The sample directions in the present work are named as follows
1) Building direction (BD): the direction of powder layer deposition, i.e., z-direction in the machine coordinate system.
2) Transverse direction (TD): in-plane direction of powder layer.
3) Normal direction (ND): in-plane direction of powder layer.

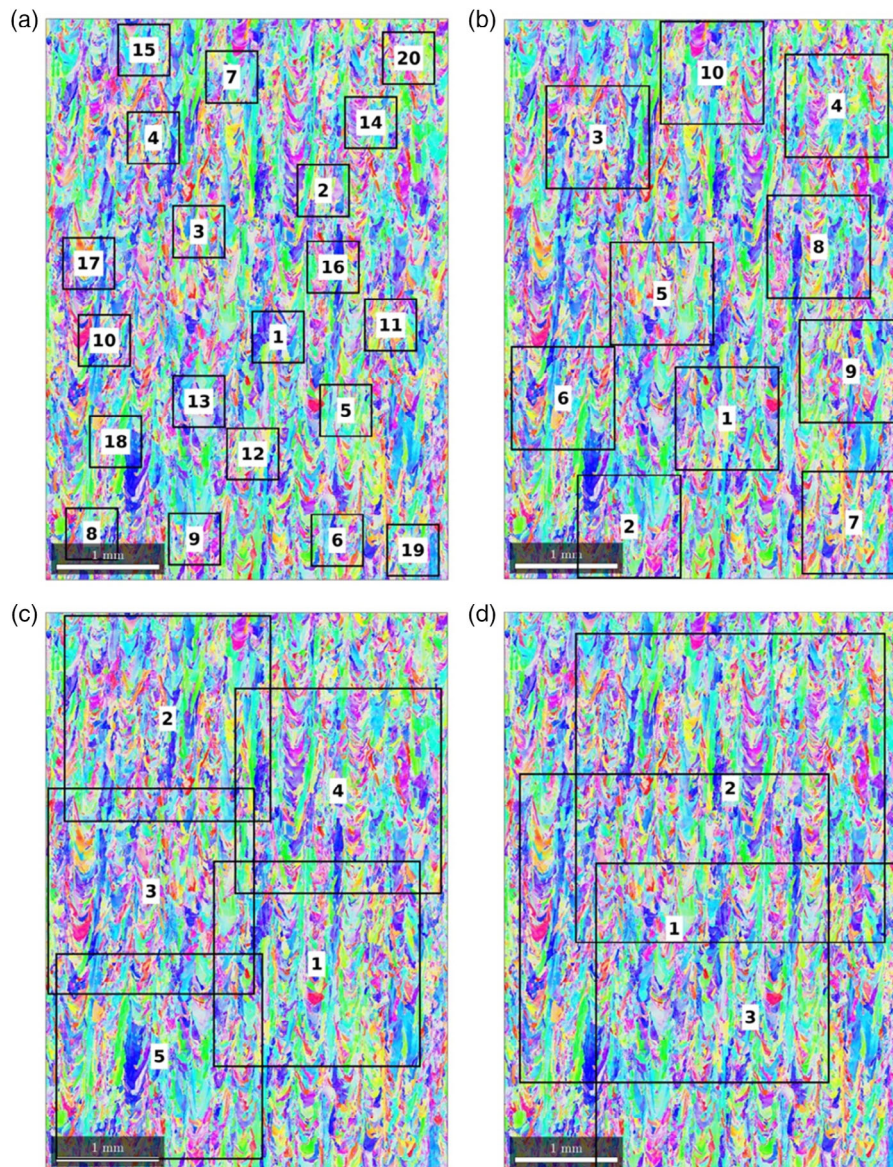


Figure 2. Multiple realizations of cropping windows of varying side lengths from the large EBSD dataset, a) 0.5 mm \times 0.5 mm cropping windows, b) 1 mm \times 1 mm cropping windows, c) 2 mm \times 2 mm cropping windows, and d) 3 mm \times 3 mm cropping windows. The numbered windows correspond to the model number in Table 1. Each extracted window was saved as a new EBSD dataset.

2.1. Sample Preparation and Setup of EBSD

From the initial manufactured block, samples were cut by electro-discharge machining (EDM). The samples are cuboid in shape with a dimension of 5 mm along BD and 4 mm along TD and ND. To prepare the sample for scanning by electron microscopy investigation, it was first ground with silicon carbide papers

and then electropolished with a Struers Lectro Pol-5 system. Good-quality samples were obtained with A2 electrolyte at 15 °C, 35 V, and 10 s polishing time. EBSD on the polished samples was conducted on JEOL JSM-F SEM operating at 30 kV with a step size of 2.96 μm (resolution of 1892 pixels in the horizontal direction [TD] and 2432 pixels in the vertical direction [BD]) and equipped with the Oxford Symmetry EBSD system.

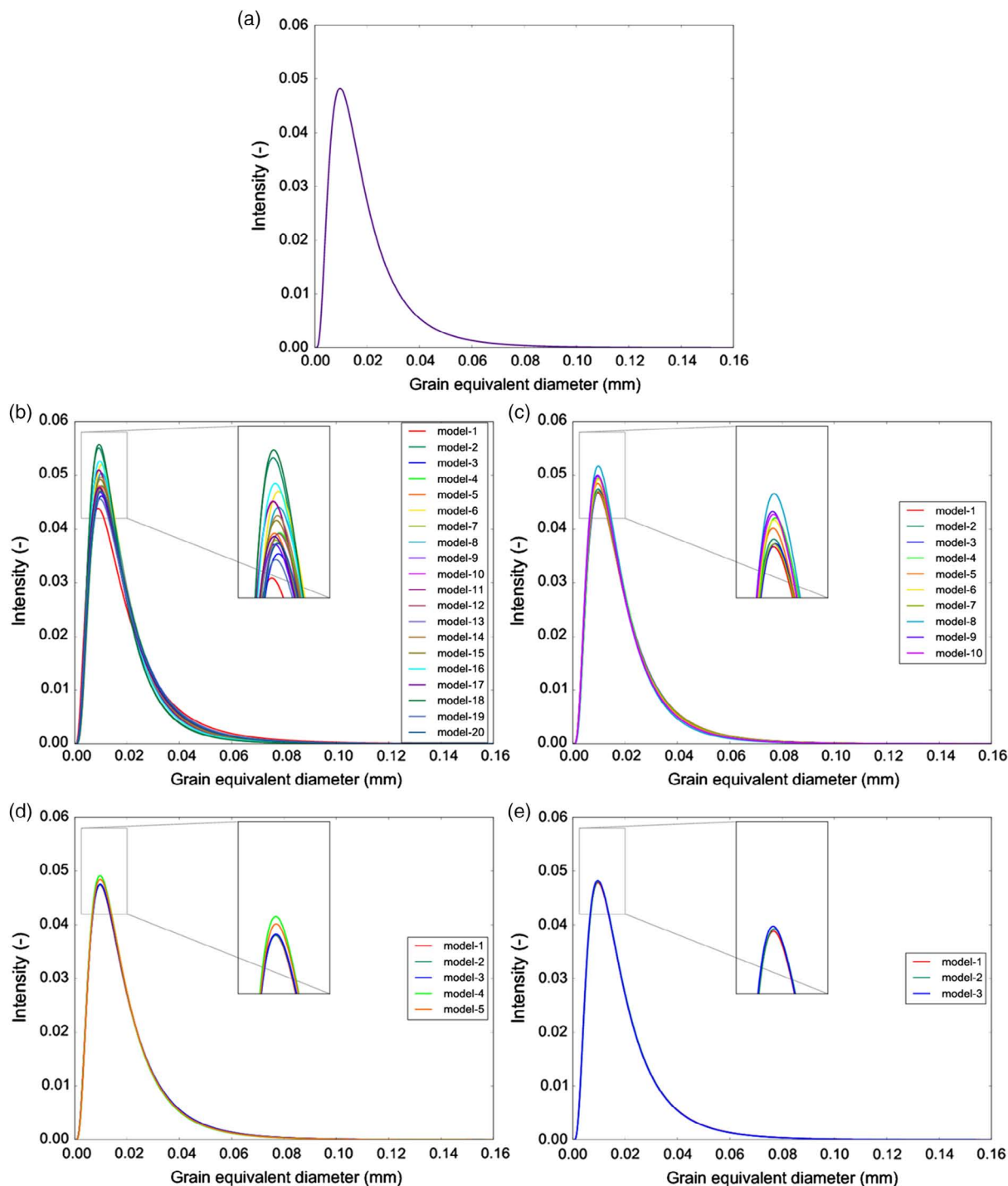


Figure 3. Grain size distribution in EBSD dataset from a) large EBSD dataset, b) cropping windows of 0.5 mm × 0.5 mm, c) cropping windows of 1 mm × 1 mm, d) cropping windows of 2 mm × 2 mm, and e) cropping windows of 3 mm × 3 mm, approximated by a log-normal distribution.

2.2. Microstructure Analysis Using EBSD

The postprocessing of the EBSD data was conducted with Mtex.^[17] The initial analysis of the EBSD data indicated the presence of noise. As suggested in the study by Hielscher et al.,^[18] the EBSD data were denoised by a filter, based on the half quadratic minimization. This provides the best possible grain reconstruction (with a threshold disorientation value of 5°) with well-defined grain boundaries. The EBSD map obtained after denoising is shown in Figure 1. Considering the observed mean equivalent grain diameter value in Table 1, grains smaller than 3 μm were excluded, and the smoothed EBSD data were used for texture estimation, which is discussed in detail in Section 3.2.

From the large EBSD map of Figure 1, small windows of side lengths 0.5, 1, 2, and 3 mm were cropped, as shown in Figure 2. The cropped windows individually represent smaller EBSD scan areas, from which the statistical data of the microstructural features were extracted. Depending on the window size, multiple realizations of a particular window were generated. Each realization was numbered, as shown in Figure 2. The average resolutions of the cropped EBSD data are 168 × 168, 337 × 337, 675 × 675, and 1013 × 1013 pixels for windows of edge lengths 0.5, 1, 2, and 3 mm, respectively. These resolutions vary within ±1 pixel in windows of each type.

From the EBSD map (Figure 1), it is evident that most of the elongated grains are oriented along the BD, which was also reported in the study by Niendorf et al.^[19] Each grain is approximated with an ellipse and the grain tilt angle which is the angle between the ellipse major axis and positive horizontal direction. From the histogram of the grain tilt angle (refer Figure S2, Supporting Information), it can be emphasized that most of the grains are aligned along the BD, which is shown by the large frequency of grain tilt angle near 90° (refer Figure 1 for sample directions).

The grain dimensions along TD and ND are assumed to be equal, and hence the grains could be approximated by ellipsoids. Considering the size of the grains, the dimension can be expressed in terms of equivalent diameter, i.e., the diameter of the circle with an area equivalent to the grain area from the EBSD map. The shape of the grains is described by their aspect ratio, i.e., the ratio of the major to the minor axes of the ellipse that represents the grain. The characterized equivalent diameter was shown to follow a log-normal distribution,^[20] and the fitted distributions for the EBSD map of Figure 1 and the cropped EBSD maps of Figure 2 are shown in Figure 3. A representation of the aspect ratio values from EBSD datasets is shown in Figure S1, Supporting Information, in form of a histogram. The mean equivalent diameter (μ_{dia}) of the log-normal distribution and the mean aspect ratio (μ_{AR}) of the grains for the various numbered windows of Figure 2 are shown in Table 1.

The range of variation observed in the characterized μ_{dia} and μ_{AR} is generally small. However, this variation is largest for the cropped EBSDs with the side length of 0.5 mm, and it reduces with the larger cropping window side length. As few grains are captured in the 0.5 mm × 0.5 mm EBSD scans, the values of μ_{dia} are largely influenced by the local grain size. With increasing EBSD scan size, this variation reduces, as the larger number of grains improves statistical estimation.

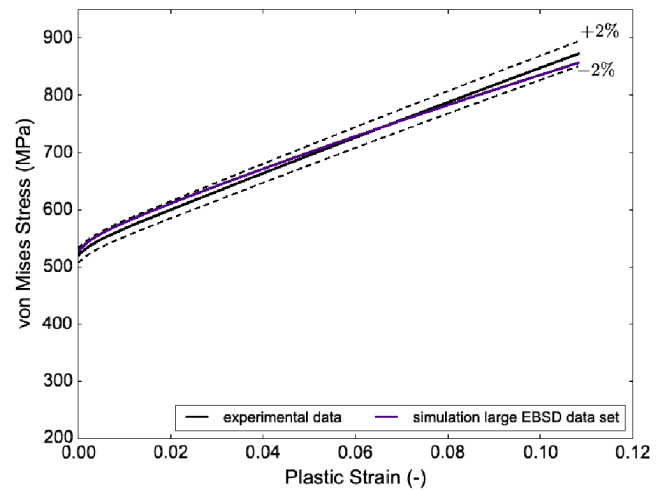


Figure 4. von Mises stress versus plastic strain plot from compression experiments and a micromechanical model of the large EBSD dataset, the dashed line represents $\pm 2\%$ of the experimental data.

2.3. Compression Test

For parameterizing the micromechanical model, we conducted a compression test at room temperature using a Zwick/Roell compression test machine with a 100 kN load cell and one Zwick/Roell extensometer of which the load was applied along BD. The sample was in a cuboid shape with a similar geometry described in Section 2.1. The test began with an initial load of 20 N and continued at a displacement rate of 0.5 mm min⁻¹ (approximate strain rate of 0.0017 s⁻¹) until reaching an engineering strain of $\approx 35\%$. The data obtained at the end of the test were in the form of engineering stress versus engineering strain, which was used to calculate the true stress versus the true strain using the classical approach given in the study by Dieter and Bacon.^[21]

The experimental data from three samples were averaged and served as reference data for the parameterization of micromechanical models (Figure 4).

3. Micromechanical Model

For predicting the mechanical response of the polycrystalline material, a micromechanical modeling approach is suggested, in which the material is approximated by a smaller, periodically repeating material element, commonly referred to as the RVE. This approximation reduces the number of degrees of freedom of the numerical problem, and at same time, it represents the material features as closely as possible. In the virtual space, the RVE can be referred to as the virtual microstructure. To incorporate the material properties, the RVE statistically imitates the geometry and the texture observed in the microstructure obtained from EBSD analysis.

3.1. RVE Generation

3.1.1. Microstructure Generator: Kanapy

To model the complexly shaped morphologies of the grains, as observed in the EBSD map of Figure 1, the in-house tool for

generating synthetic microstructures, Kanapy^[22] was used. From EBSD characterization, the equivalent diameter, the aspect ratio, and the tilt angle of the grains are extracted and used as input for RVE generation. Kanapy generates ellipsoidal particles, that represent elongated grains, following the provided size distribution, and packs these particles into a simulation box, which represents the final RVE. During the packing process, the particles interact with each other and with the simulation box. The interaction between the particles is modeled by breaking it down into stages of collision detection and response. The interaction between the particles and the simulation box can be modeled by evaluating whether the particles cross the boundaries of the box. If periodicity is enabled, periodic images on the opposite boundaries of the box are created; otherwise, the particle position and velocity vectors have to be updated to mimic the bouncing-back effect.

For collision detection, the algebraic separation condition developed by Wang et al.^[23] is used to determine whether two static ellipsoids overlap. If collision is established, the particles bounce back and continue their motion in opposite directions. As each particle has to be checked for collision with every other particle in the domain, the approach can be computationally expensive. To overcome this, a two-layer collision detection scheme using an octree spatial partitioning data structure^[24,25] and a bounding sphere hierarchy^[26] is implemented within Kanapy. The general framework of collision detection response systems with two-layer spatial-partitioning data structures has the following features: 1) Recursive decomposition of the given domain into subdomains based on the octree data structure. 2) Performance of collision tests between bounding spheres of ellipsoids belonging to the same subdomain. 3) Tests for ellipsoid overlap condition only if the bounding spheres overlap. 4) Update of the position and the velocity vectors based on the collision response. 5) Test for collision with the simulation domain and creation of periodic images on the opposite boundaries or mimicking the bouncing-back effect.

For a more detailed description regarding the collision detection scheme and its implementation, kindly refer to the study by Prasad et al.^[22] The packing simulation terminates itself once the ellipsoidal particles are tightly packed with minimum acceptable overlaps. As the ellipsoidal particles are defined by their major and their minor diameters, classical Voronoi tessellation cannot be used here.

Kanapy has a voxel-based mesh-generating routine that can populate the RVE with voxels and assign these voxels to the respective particles based on their position and dimensions. The generated hexahedral mesh (C3D8 elements) can be read by the commercial FE software ABAQUS.^[27] Based on the parameters describing grain size distribution and shape statistics as obtained from the EBSD of Figure 1 and the cropped EBSDs from Figure 2, five RVEs consisting of 1000 grains were generated with Kanapy. These RVEs are shown in Figure 5. The statics of the grain dimensions in RVE is shown in Table S1, Supporting Information, of which they are in good agreement with experimental data shown in Table 1.

3.2. Texture Representation

The crystallographic texture can be represented in the form of a continuous function known as the ODF.^[28] The ODF is

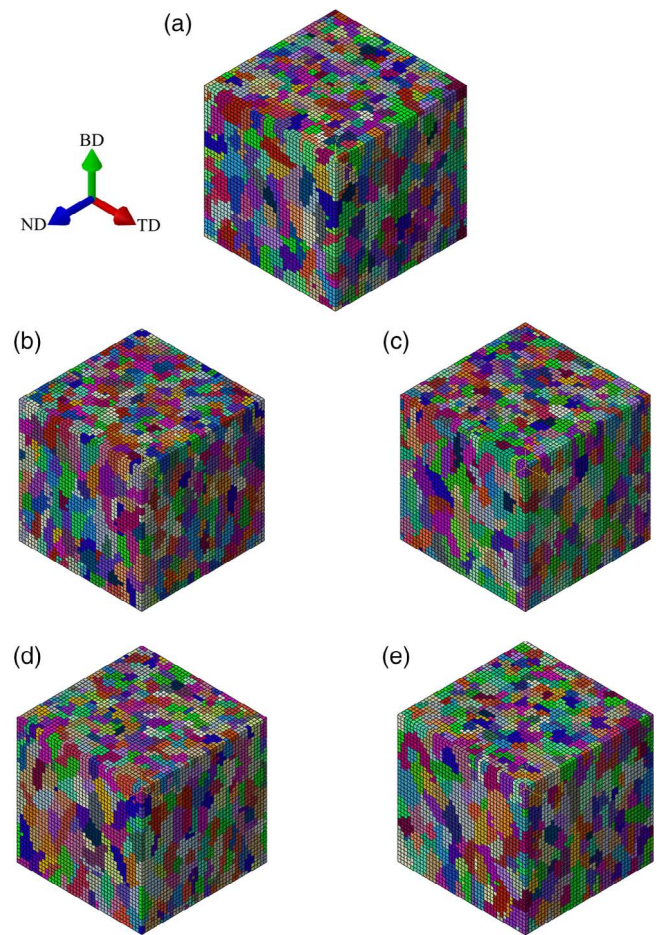


Figure 5. Polycrystalline RVEs (consisting of 1000 grains) generated with Kanapy, depicting elongated grains as observed in the EBSD map along BD. The RVEs of cubic shape are generated from the following EBSD datasets a) large EBSD dataset (RVE edge length = 0.133 mm), b) cropping windows 0.5 mm × 0.5 mm (RVE edge length = 0.161 mm), c) cropping windows 1 mm × 1 mm (RVE edge length = 0.162 mm), d) cropping windows 2 mm × 2 mm (RVE edge length = 0.162 mm), and e) cropping windows 3 mm × 3 mm (RVE edge length = 0.147 mm).

estimated by the convolution of the bell-shaped de la Valeé kernel function placed at the experimentally measured orientations. This kernel is chosen as it is a non-negative kernel with finite Fourier series expansion, which is specially advantageous for ODF estimation. Further details regarding this can be found in the study by Schaeben.^[29]

The ODF (\varnothing) representing the crystallographic texture can be estimated on $\varnothing: SO(3) \rightarrow \mathbb{R}$ from the crystallographic orientation measurements g_i , where $i = 1, \dots, N$, based on a kernel function $\Psi: [0, \pi] \rightarrow \mathbb{R}$.^[30]

$$\varnothing(g) = \frac{1}{N} \sum_{i=1}^N \Psi(\omega(g_i^{-1}g)), \quad g \in SO(3) \quad (1)$$

where $\omega(g_i^{-1}g)$ is the disorientation between g_i and g . For the sake of computational feasibility, the ODF has to be reconstructed with a smaller number (N') of discrete orientations (g'_i).

Considering all g'_i as equally weighted, the reconstructed ODF (φ') can be represented as

$$\varphi'(g) = \frac{1}{N} \sum_{i=1}^N \Psi(\omega(g'_i^{-1}g)), \quad g \in SO(3) \quad (2)$$

Therefore, the L^1 error between the ODFs can be estimated as

$$L_1^{\text{ODF}} = \|\varphi - \varphi'\|_1 = \int_{SO(3)} |\varphi(g) - \varphi'(g)| dg \quad (3)$$

The grain size in RVE is restricted within a small variation from the mean value, and it is thus assumed that the ODF represented by RVE (considering the grain volume fraction)

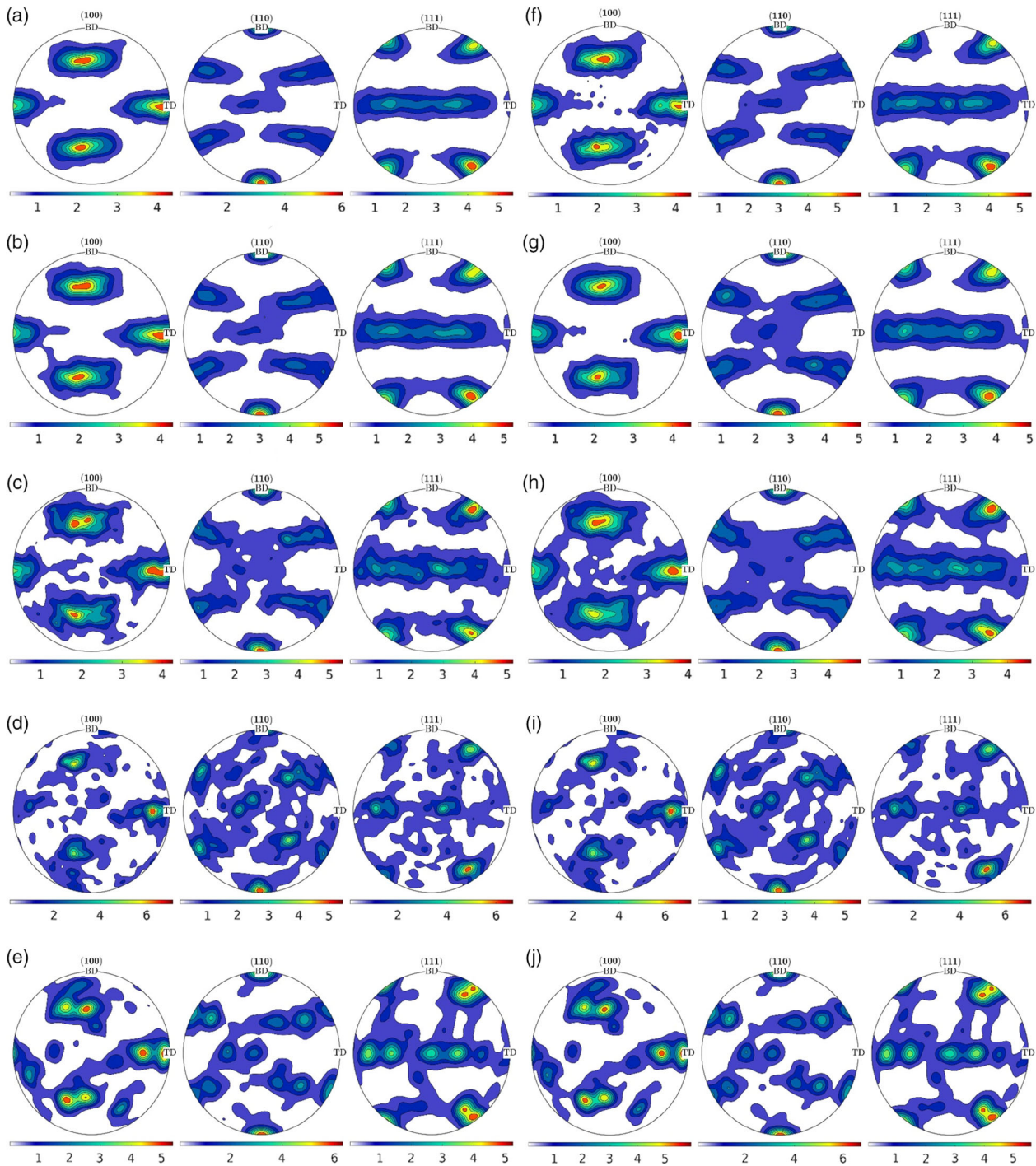


Figure 6. Pole figures for the ODFs-estimated EBSD datasets shown in a) large EBSD dataset, b) 3 mm × 3 mm EBSD dataset (model 1), c) 2 mm × 2 mm EBSD dataset (model 3), d) 1 mm × 1 mm EBSD dataset (model 7), e) 0.5 mm × 0.5 mm EBSD dataset (model 16), and the respective reconstructed ODFs from orientations are shown in (f–j), respectively.

can be estimated by considering all the orientations as equally weighted. The reconstruction process using discrete orientations is conducted using a L_1^{ODF} minimization scheme,^[31] and the algorithm is terminated in case a value less than 0.1 is achieved. In the extreme case, when the ODFs \emptyset and \emptyset' are concentrated around disjoint orientations, L_1^{ODF} approaches 2.

The results of the ODF reconstruction are demonstrated in the form of pole figure contour plots. From Figure 1 and 2, for each size of the EBSD cropping window, one realization is selected, and its ODF along with the reconstructed ODFs are shown for comparison in Figure 6. Figure 6a–e shows the ODF estimated from the large EBSD scan as well as the EBSD from cropping windows, and the corresponding reconstructed ODFs estimated from 1000 discrete orientations are shown in Figure 6f–j. More examples of such reconstructions with application of CPFEM can be found in the study by Biswas et al.^[31]

The comparison in Figure 6 shows successful ODF reconstruction, as the contour plots of the reconstructed and the input ODF show similar peak locations with intensity values. Furthermore, L_1^{ODF} from the ODF reconstruction results for all the EBSDs are shown in Table 2, of which values are relatively low. In addition to the crystallographic texture, polycrystalline materials also have a grain boundary texture which can be represented in the form of the grain boundary disorientation angle distribution. To mimic this distribution, orientations can be systematically assigned to the RVE grains using the algorithm suggested in the study by Biswas et al.^[32]

Table 2. ODF reconstruction results with discrete orientations, the values represent L_1^{ODF} .

Model	Large EBSD scan	3 mm × 3 mm	2 mm × 2 mm	1 mm × 1 mm	0.5 mm × 0.5 mm
1	0.057	0.077	0.094	0.068	0.038
2		0.073	0.096	0.067	0.038
3		0.075	0.096	0.067	0.057
4			0.097	0.069	0.043
5			0.097	0.065	0.039
6				0.095	0.065
7				0.098	0.050
8				0.074	0.062
9				0.066	0.053
10				0.066	0.061
11					0.059
12					0.045
13					0.041
14					0.058
15					0.041
16					0.046
17					0.057
18					0.053
19					0.045
20					0.059

3.3. Micromechanical Model and Homogenization Scheme

This section presents a brief description of the CP model used to reproduce the plastic deformation in the RVE in the FE framework. For a detailed description please refer to the studies by Ma and Hartmaier and Roters et al.^[33,34] and the references therein. Please note that in this work, the effects of the plastic strain gradient are not considered. The total deformation gradient \mathbf{F} is multiplicatively decomposed into an elastic part \mathbf{F}^e representing a reversible lattice deformation and a plastic part \mathbf{F}^p representing an irreversible lattice deformation. Thus

$$\mathbf{F} = \mathbf{F}^e \mathbf{F}^p \quad (4)$$

The evolution of plastic deformation is captured as

$$\dot{\mathbf{F}}^p = \mathbf{L}^p \mathbf{F}^p \quad (5)$$

where \mathbf{L}^p is the plastic velocity gradient. As the plastic deformation is defined by the dislocation motion on active slip systems, \mathbf{L}^p is expressed as the sum of the shear rate $\dot{\gamma}_\alpha$ at each slip system α . Therefore for N_s slip systems \mathbf{L}^p is expressed as

$$\mathbf{L}^p = \sum_{\alpha=1}^{N_s} \dot{\gamma}_\alpha \mathbf{M}^\alpha \quad (6)$$

\mathbf{M}^α (known as the “Schmid tensor”) is expressed in terms of the slip direction \mathbf{d}^α and the slip plane normal \mathbf{n}^α as $\mathbf{M}^\alpha = \mathbf{d}^\alpha \otimes \mathbf{n}^\alpha$.

In this work, the “phenomenological constitutive model” is used, and in this framework, the aforementioned $\dot{\gamma}_\alpha$ is formulated as

$$\dot{\gamma}_\alpha = \dot{\gamma}_0 \left| \frac{\tau^\alpha}{\hat{\tau}^\alpha} \right|^{p_1} \text{sgn}(\tau^\alpha) \quad (7)$$

where $\dot{\gamma}_0$ is the reference shear rate, p_1 is the inverse of the strain rate sensitivity, and τ^α is the resolved shear stress, which is the mapped stress due to elastic strain $\left(\frac{1}{2} (\mathbf{F}^{eT} \mathbf{F}^e - \mathbf{I}) \right)$ on the slip systems

$$\tau^\alpha = \frac{\mathbb{C}}{2} (\mathbf{F}^{eT} \mathbf{F}^e - \mathbf{I}) \cdot \mathbf{M}^\alpha \quad (8)$$

where \mathbb{C} represents the stiffness matrix. The slip resistance $\hat{\tau}^\alpha$ describes the hardening behavior of the material and it is expressed as

$$\hat{\tau}^\alpha = \sum_{\beta=1}^{N_s} h_0 \chi_{\alpha\beta} \left(1 - \frac{\hat{\tau}^\beta}{\hat{\tau}_f} \right)^{p_2} |\dot{\gamma}_\beta| \quad (9)$$

which starts from an initial value of $\hat{\tau}^\alpha$ and the other parameters are h_0 the hardening rate, $\chi_{\alpha\beta}$ the cross-hardening matrix in which the diagonal elements representing the coplanar slip systems are set to 1.0 and off-diagonal elements representing the noncoplanar slip systems are set to 1.4, $\hat{\tau}_f$ the saturation slip resistance due to dislocation accumulation, and p_2 a fitting parameter. As 316L stainless steel belongs to the family of austenitic stainless steels (face-centered cubic [FCC] crystalline structure),

Table 3. Optimized CP parameters from FEM simulations.

Parameter	Value [MPa]
$C_{11}^{[36]}$	164 000
$C_{12}^{[36]}$	110 000
$C_{44}^{[36]}$	101 000
$\dot{\gamma}_0$	0.001 s^{-1}
p_1	85
p_2	2.5
σ_0^a	200
$\hat{\tau}_f$	1123
h_0	600

the dislocation in such crystalline metals moves on 12 slip systems that can be defined using Miller indices as $\{110\}\langle 111\rangle$.

The RVE is modeled so that it is periodic in all directions. To implement periodic boundary conditions, the boundary nodes of opposite faces are constrained by equations which maintain the RVE's structural periodicity even in the deformed state. Furthermore, the results from the RVE are averaged with an energetically consistent scheme utilizing reaction forces and

position vectors of the boundary nodes. The details and the implementation of the periodic boundary condition and the averaging scheme can be found in the study by Vajragupta et al.^[35]

To parameterize the CP model, the RVE generated from the large EBSD dataset was used with a CP model through UMAT (user defined material subroutine) and simulated in ABAQUS^[27] under a compression loading condition. The CP parameters were systematically adapted to match the homogenized stress–strain curve with the experimental result. With optimized CP parameters shown in Table 3, the compression simulation result of the parameterized micromechanical model was in good agreement with the experimental data, as shown in Figure 4.

4. Results and Discussion

4.1. EBSD Analysis Results

Because the microstructural features like texture and grain size play an important role in micromechanical simulations, they were used for comparing, smaller cropped EBSD datasets with the large EBSD dataset. The comparison provided an insight into how the results predicted by the CPFEM were affected by the change of these features, which were by themselves influenced by a smaller

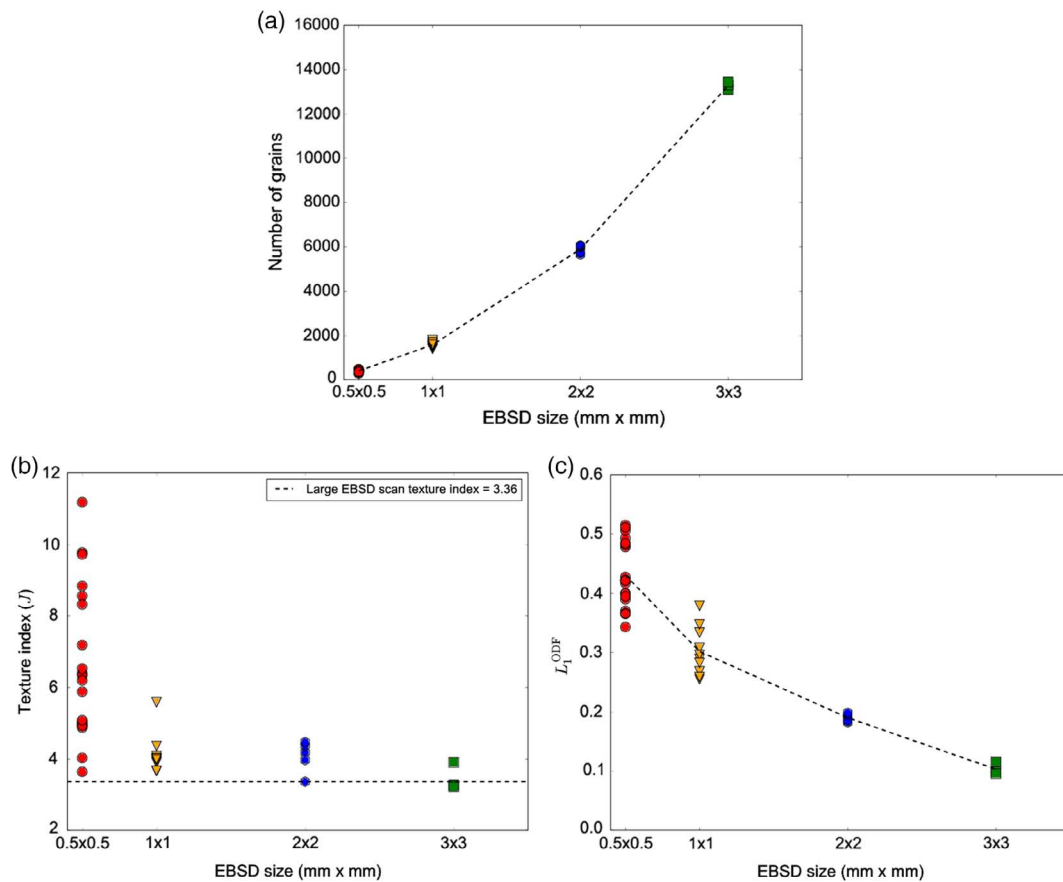


Figure 7. The comparison of a) number of grains captured in each of the cropped EBSD windows is plotted against the corresponding EBSD size, b) texture index for each of the cropped EBSD windows is plotted against the corresponding EBSD size, c) L_1^{ODF} for each of the cropped EBSD datasets is plotted against the corresponding EBSD size.

scan area. The ODF of the large EBSD dataset and the ODF of the cropped EBSD datasets were compared using the texture index^[37]

$$J = \int_{SO(3)} [\varnothing(g)]^2 dg \quad (10)$$

and the L_1^{ODF} error is described in Equation (3).

Figure 7a shows the comparison of the number of grains in the cropped EBSD datasets. The number of grains for each cropping window size is as follows: 0.5 mm × 0.5 mm: 283–479, 1 mm × 1 mm: 1401–1787, 2 mm × 2 mm: 5652–6058, and 3 mm × 3 mm: 13 099–13 430.

The comparison of L_1^{ODF} between all cropped EBSD datasets is shown in Figure 7c. This figure indicates a large variation in the data estimated for various 0.5 mm × 0.5 mm models, and as the EBSD scan size increases, the variations reduces. As the ODF is a kernel density estimate that indicates the probability of finding a crystallographic orientation per unit volume, larger input datasets would lead to a better ODF estimation. Ultimately, this can be correlated with the number of grains captured by the EBSD. This effect can also be observed in the contour plot of the pole figures from the large EBSD dataset (shown in Figure 6a) and the cropped EBSD datasets (shown in Figure 6b–e). The pole figure from 0.5 mm × 0.5 mm EBSD (Figure 6e) and the large EBSD dataset (Figure 6a) shows a significant difference.

A similar trend is observed in the comparison of the texture index shown in Figure 7b. Even though the EBSD scan is performed on a polycrystalline material, cropped EBSD scans capturing very few grains with similar orientations may represent an approximate single crystal material (indicated by the high texture index in Figure 7b and the number of grains in Figure 7a).

4.2. Micromechanical Simulation Results

In this section, the mechanical response of the material under compression load is presented in the form of stress–strain plots. Figure 8 shows the plastic strain versus the von Mises stress from simple compression tests of the RVE generated with the large EBSD scan. The experimental data shown in this figure are used for the calibration of CP parameters, and the result for the same is shown in Figure 4. The results from the cropped EBSD datasets of window size 0.5 mm × 0.5 mm show a large scatter, which reduces with increasing EBSD window size. Furthermore, this scatter in results can be correlated with the scatter in texture obtained from the cropped EBSD datasets (please refer to Figure 7b), which is maximum for EBSDs with 0.5 mm × 0.5 mm cropping window size. The difference in texture has a substantial influence on the crystallographic orientations assigned to the RVE grains, which affect the results of the CPFEM.

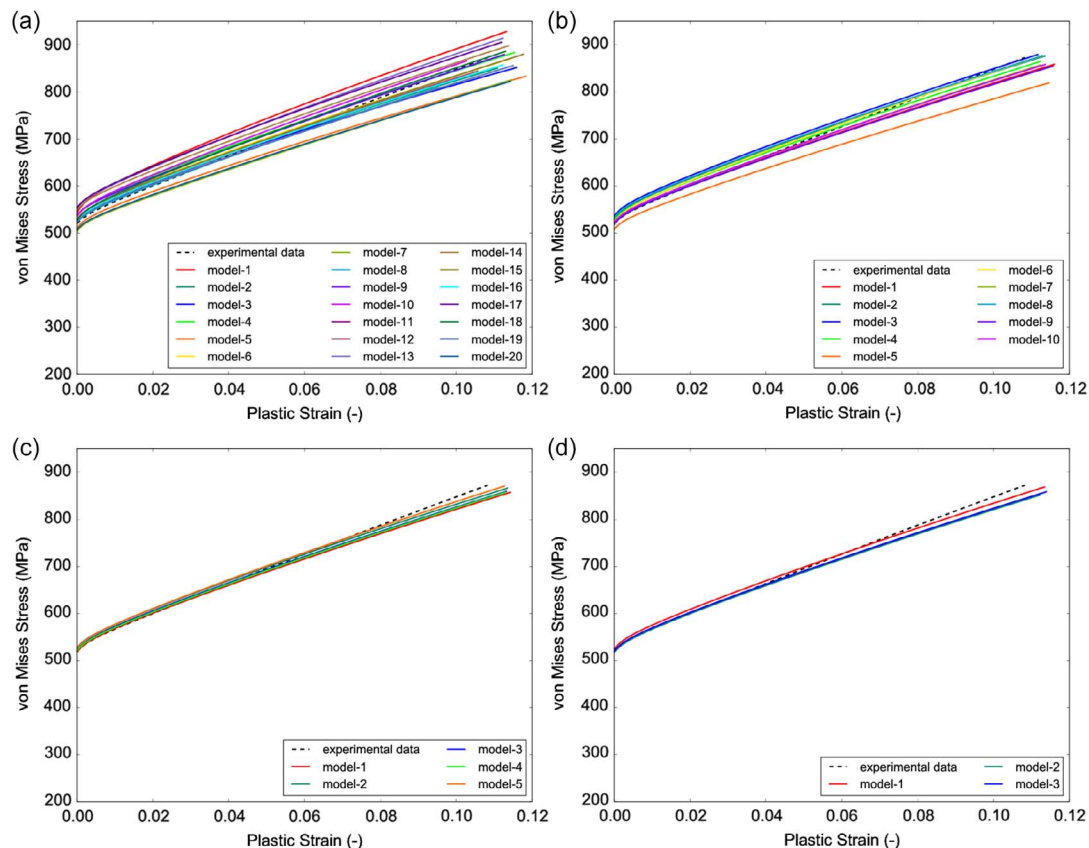


Figure 8. von Mises stress versus plastic strain plot for the micromechanical models generated from cropped EBSD datasets with windows of sizes: a) 0.5 mm × 0.5 mm, b) 1 mm × 1 mm, c) 2 mm × 2 mm, and d) 3 mm × 3 mm (refer Figure 2 for the EBSD map). Not all the lines in results may be visible due overlapping of data.

A more detailed study of the local stresses, in form of von Mises stress calculated at element integration points, is shown in **Figure 9**. The stress data are represented in the form of a probability density function (f_i^{j2}) where i is the model number of the cropped EBSD dataset of Figure 2. This density is estimated from a histogram with a bin width of ≈ 2.5 MPa; therefore, the probability of the data in the j th bin ranging from σ_j and $\sigma_j + d\sigma$ ($d\sigma = 2.5$) is

$$P_j = \lambda_j / \Gamma \quad (11)$$

where λ_j is the number of data samples within the range σ_j and $\sigma_j + d\sigma$ and Γ is the total number of data samples. Therefore, the probability density function at any stress value σ_j can be expressed as

$$f_i^{j2}(\sigma_j) = \frac{P_j}{d\sigma} \quad (12)$$

Similarly, the von Mises stress probability density function for the RVE simulation generated from the large EBSD dataset (f_{ref}^{j2})

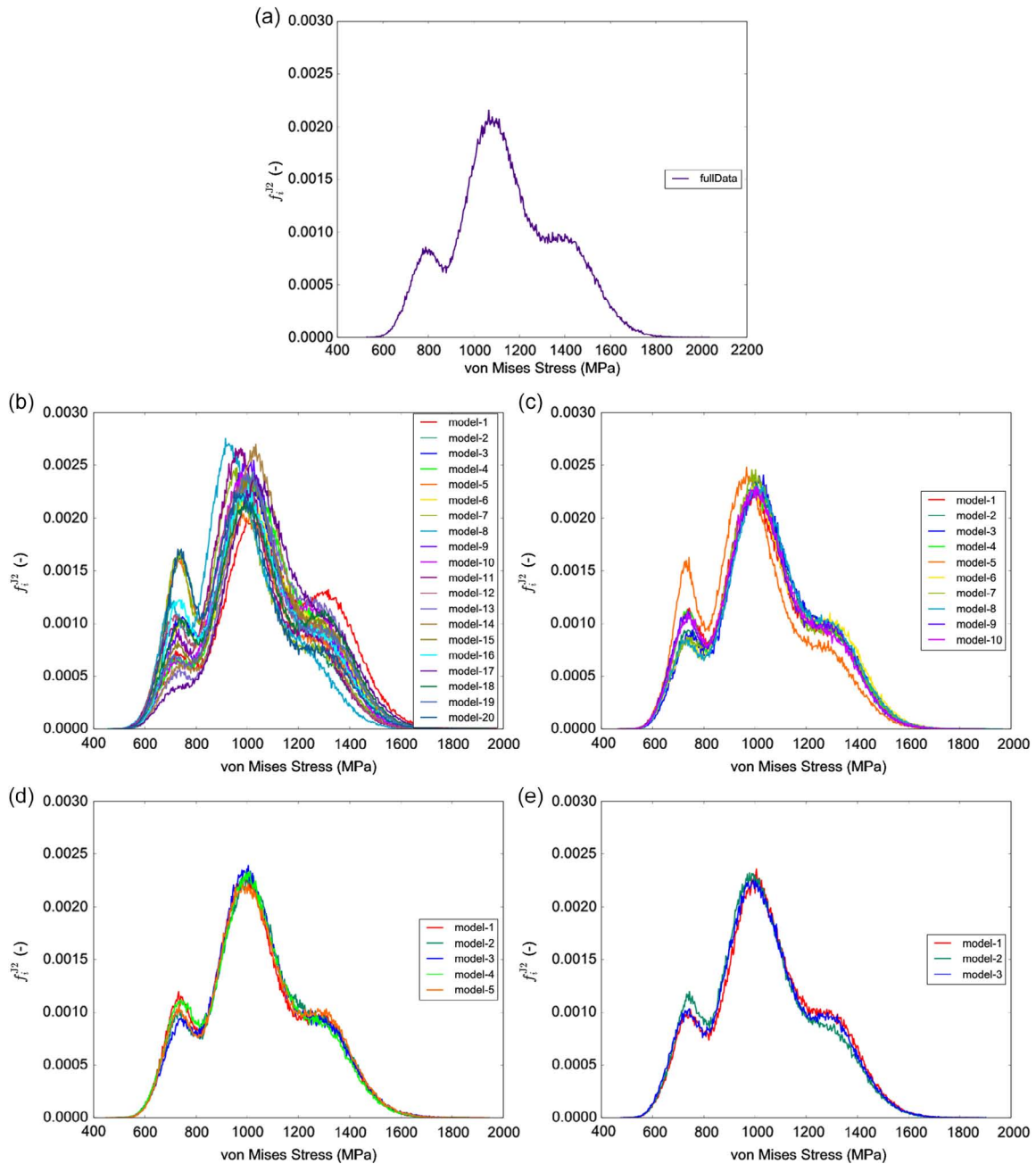


Figure 9. Probability density function (f_i^{j2}) of the von Mises stress calculated at each integration point of the FE in the micromechanical model generated from the following EBSD datasets: a) large scan, b) $0.5 \text{ mm} \times 0.5 \text{ mm}$ cropping windows, c) $1 \text{ mm} \times 1 \text{ mm}$ cropping windows, d) $2 \text{ mm} \times 2 \text{ mm}$ cropping windows, and e) $3 \text{ mm} \times 3 \text{ mm}$ cropping windows.

is taken as reference and compared with the results from the cropped EBSDs using the L_1 norm

$$L_1^{J2} = \left\| f_{ref}^{J2} - f_i^{J2} \right\|_1 \quad (13)$$

(Figure 10). Similar to the results in the stress–strain plots, a large variation is seen in the results for the 0.5 mm × 0.5 mm cropped EBSD datasets, which reduces with the size of the cropping window.

On the other hand, averaging all the results (i.e., von Mises stresses) from the cropping window of each size approximates the result from the large EBSD dataset closely (refer to Figure 11). This can be used as an effective strategy to incorporate experimental data into modeling, in which several montages of EBSD scans can be conducted at different locations and then

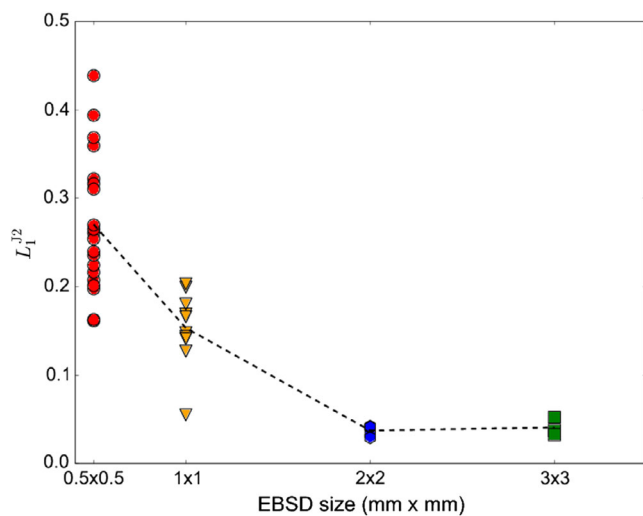


Figure 10. A comparison of L_1^{J2} calculated using von Mises stress from the micromechanical model generated from a large EBSD dataset and cropped EBSD datasets.

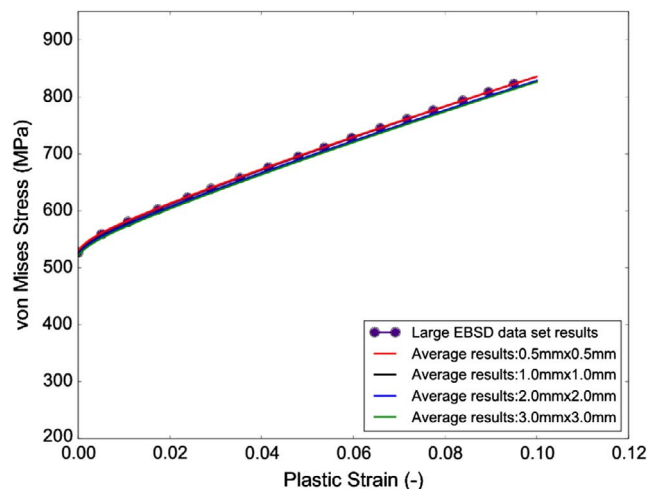


Figure 11. A comparison of the averaged von Mises stress versus plastic strain results from all the cropped EBSD datasets (belonging to each window size) with the large EBSD datasets.

combined to form a collective experimental dataset for predicting the global material behavior. This strategy can be useful in many cases like experimental setup limitations or a graded microstructure. However, such an averaging method may overlook local deformation behavior in a graded microstructure.

5. Conclusions

This work concentrated on the effect of the EBSD scan area on the results of a micromechanical model and provided an insight into the proper integration of experiments into modeling. It was found that the number of grains captured in the analysis, rather than the scanned area, provides a suited parameter for judging the validity of the derived statistical quantities to characterize the microstructure. To conduct this study, small EBSD datasets were obtained by cropping a large EBSD dataset. The variation in the results obtained from the smaller EBSD datasets shows the importance of a sufficiently large dataset from experiments for modeling. As the scan area is reduced, the number of grains captured by the EBSD also reduces, and the scatter in the derived statistical data increases. Hence, because the micromechanical model is a statistical derivative of the experiments, a large scatter in the results from the micromechanical models is observed. This scatter is also reflected in the error in texture estimation from the cropped EBSDs.

Individually, the results from the cropped EBSD datasets are not sufficient for modeling. However, the average of the results obtained from the models of the cropped EBSD approximates the results from a large EBSD dataset in a very good way. Based on these results, there can be two different modeling strategies: first, a single large EBSD dataset covering more than 10 000 grains (which is also observed in the experimental study^[9]) can be used to derive a proper statistical description of the microstructure and second, several montages from different locations of the sample can be combined into unified experimental datasets and then used for modeling. There can be several factors ranging from limitations in the experimental setup to a complex microstructure, which can govern the choice of the most appropriate modeling strategy.

Supporting Information

Supporting Information is available from the Wiley Online Library or from the author.

Acknowledgements

The authors acknowledge ZGH (Center for Interface-Dominated High Performance Materials [Zentrum für Grenzflächendominierte Höchstleistungswerkstoffe] RUB) for granting access to the SEM/EBSD system used in this study. A.B. gratefully acknowledges funding from IMPRS-SurMat. T.N. acknowledges funding provided by DFG (project no. 250216343).

Conflict of Interest

The authors declare no conflict of interest.

Keywords

additive manufacturing, electron backscatter diffraction, micromechanical modelings, 316L stainless steels

Received: December 3, 2019
Revised: February 14, 2020
Published online: March 5, 2020

- [1] R. J. M. Smit, W. A. M. Brekelmans, H. E. H. Meijer, *Comput. Method Appl. Mech. Eng.* **1998**, 155, 181.
- [2] S. R. Kalidindi, C. A. Bronkhorst, L. Anand, *J. Mech. Phys. Solids* **1992**, 40, 537.
- [3] G. B. Sarma, P. R. Dawson, *Int. J. Plast.* **1996**, 12, 1023.
- [4] A. J. Beaudoin Jr, H. Mecking, U. F. Kocks, *Philos. Mag. A* **1996**, 73, 1503.
- [5] A. Ahmadi, R. Mirzaeifar, N. S. Moghaddam, A. S. Turabi, H. E. Karaca, M. Elahinia, *Mater. Des.* **2016**, 112, 328.
- [6] M. T. Andani, M. R. Karamooz-Ravari, R. Mirzaeifar, J. Ni, *Mater. Des.* **2018**, 137, 204.
- [7] F. J. Humphreys, *Scr. Mater.* **2004**, 51, 771.
- [8] V. Randle, O. Engler, *Introduction To Texture Analysis: Microtexture, Microtexture And Orientation Mapping*, CRC Press, Boca Raton, FL **2014**.
- [9] S. I. Wright, M. M. Nowell, J. F. Bingert, *Metall. Mater. Trans. A* **2007**, 38, 1845.
- [10] J. Jura, J. Pospiech, G. Gottstein, *Z. Metallkd.* **1996**, 87, 476.
- [11] K. Davut, S. Zaeferrer, *Metall. Mater. Trans. A* **2010**, 41, 2187.
- [12] E. Nakamachi, N. N. Tam, H. Morimoto, *Int. J. Plast.* **2007**, 23, 450.
- [13] D. Brands, D. Balzani, L. Scheunemann, J. Schröder, H. Richter, D. Raabe, *Arch. Appl. Mech.* **2016**, 86, 575.
- [14] H. Zhang, M. Diehl, F. Roters, D. Raabe, *Int. J. Plast.* **2016**, 80, 111.
- [15] C. Pélissou, J. Baccou, Y. Monerie, F. Perales, *Int. J. Solids Struct.* **2009**, 46, 2842.
- [16] A. Riemer, S. Leuders, M. Thöne, H. A. Richard, T. Tröster, T. Niendorf, *Engineering Fracture Mechanics* **2014**, 120, 15.
- [17] F. Bachmann, R. Hielscher, H. Schaeben, in *Solid State Phenomena* (Eds: H. Klein, R. A. Schwarzer), Vol. 160, Trans Tech Publications, Switzerland **2010**, 63.
- [18] R. Hielscher, C. B. Silbermann, E. Schmidl, J. Ihlemann, *J. Appl. Crystallogr.* **2019**, 52, 984.
- [19] T. Niendorf, S. Leuders, A. Riemer, H. A. Richard, T. Tröster, D. Schwarze, *Metall. Mater. Trans. B*, **2013**, 44, 794.
- [20] M. Groeber, S. Ghosh, M. D. Uchic, D. M. Dimiduk, *Acta Mater.* **2008**, 56, 1257.
- [21] G. E. Dieter, D. J. Bacon, *Mechanical Metallurgy*, Vol. 3, McGraw-Hill, New York **1986**.
- [22] M. R. G. Prasad, N. Vajragupta, A. Hartmaier, *J. Open Source Softw.* **2019**, 4, 43.
- [23] W. Wang, J. Wang, M.-S. Kim, *Comput. Aided. Geom. Des.* **2001**, 18, 531.
- [24] D. Meagher, *Comput. Gr. Image Process.* **1982**, 19, 129.
- [25] H. Noborio, S. Fukuda, S. Arimoto, *Adv. Robot.* **1988**, 3, 193.
- [26] J. T. Klosowski, M. Held, J. S. B. Mitchell, H. Sowizral, K. Zikan, *IEEE Trans. Vis. Comput. Gr.* **1998**, 4, 21.
- [27] Dassault Systemes, *Abaqus* **2012**, <http://www.3ds.com/products-services/simulia/products/abaqus/>.
- [28] U. F. Kocks, C. N. Tomé, H.-R. Wenk, *Texture And Anisotropy: Preferred Orientations In Polycrystals And Their Effect On Materials Properties*, Cambridge University Press, Cambridge, UK **2000**.
- [29] H. Schaeben, *Phys. Status Solidi B* **1997**, 200, 367.
- [30] R. Hielscher, *J. Multivar. Anal.* **2013**, 119, 119.
- [31] A. Biswas, N. Vajragupta, R. Hielscher, A. Hartmaier, *J. Appl. Cryst.* **2020**, 53, 178.
- [32] A. Biswas, M. R. G. Prasad, N. Vajragupta, H. ul. Hassan, F. Brenne, T. Niendorf, A. Hartmaier, *Adv. Eng. Mater.* **2019**, 21, 1900275.
- [33] A. Ma, A. Hartmaier, *Philos. Mag.* **2014**, 94, 125.
- [34] F. Roters, P. Eisenlohr, L. Hantcherli, D. D. Tjahjanto, R. B. Thomas, D. Raabe, *Acta Mater.* **2010**, 58, 1152.
- [35] N. Vajragupta, S. Ahmed, A. Ma, M. Boeff, A. Hartmaier, *Phys. Mesomech.* **2017**, 20, 343.
- [36] H. M. Ledbetter, *Elastic Constants of Stainless Steels 304, 310, and 316 between 4 and 295 k* (Ed: R. P. Reed), Technical Report (NBSIR-80-1627), United States **1980**.
- [37] H.-J. Bunge, *Texture Analysis In Materials Science: Mathematical Methods*, Elsevier, Amsterdam, Netherlands **2013**.